Study on the Slippage and Thermodynamic Synthetic Effects on the Seepage Transport Model for Multi-Branch Coal Seam Gas Extraction Borehole Parameter Optimization

Qi Zhang , Jinlong Jia * , Zhengyuan Qin , Qiusheng Wang

Posted Date: 15 April 2026

doi: 10.20944/preprints202604.1030.v1

Keywords: thick and high-gas seams; slippage effect; dynamic viscosity; branch length; sub-major branch angle; thermal–fluid–structure coupling

 doi:10.20944/preprints202604.1030.v1

Article

Study on the Slippage and Thermodynamic Synthetic Effects on the Seepage Transport Model for Multi-Branch Coal Seam Gas Extraction Borehole Parameter Optimization

Qi Zhang [1], Jinlong Jia [1,*], Zhengyuan Qin [1] and Qiusheng Wang [2]

[1] School of Resources and Safety Engineering, Wuhan Institute of Technology, Wuhan 430205, China

[2] The First Geological Brigade of Hubei Geological Bureau, Hubei Huangshi

* Correspondence: cumt7755@126.com

Abstract

The application of multi-branch pinnate drilling has great prospects in gas control. Although there are many studies on the parameters of multi-branch plume drilling, the mathematical model used in the study is still not sufficient for the addition of the slippage effect and thermodynamic changes. In this paper, a thermal–fluid–solid coupling model is used to study the influence of branch angle and branch length on the extraction effect in high-gas and extra-thick coal seams. The reliability of the model is verified by simulating an onsite extraction environment to fit the onsite gas production rate. Under identical simulation conditions, the experiment investigated the gas extraction performance of boreholes with varying branch angles (30°, 40°, 50°, and 60°) and branch lengths (50 m, 75 m, 100 m, and 125 m). The results show that temperature affects the dynamic viscosity of gas, which in turn affects the flow rate. The slippage effect affects permeability. When the branch angle is less than 50°, the increase in the branch angle can expand the control range of drilling. By continuing to increase the angle, the improvement in the extraction effect is weakened. As the branch angle exceeds 50° and continues to increase, the branch borehole progressively approaches the edge of the coal seam. At this time, the overall control range of the borehole is greatly increased, and the gas extraction effect is improved. The increase in the branch length leads to a considerable improvement in the extraction effect. When the branch length is below 100 m, the improvement in extraction efficiency diminishes progressively with increasing branch length. This is because the effect of increasing the branch length on improving the overall control range of the borehole is weakened. When the branch length exceeds 100 m and continues to increase, the branch borehole approaches the edge of the coal seam. The overall control effect of drilling has been greatly improved. The extraction effect of boreholes has increased significantly compared with before.

Keywords: thick and high-gas seams; slippage effect; dynamic viscosity; branch length; sub-major branch angle; thermal–fluid–structure coupling

1. Introduction

The process of coal mining is associated with a number of hazards, with the primary risk being the presence of coalbed methane, also known as gas (CH_4). In the process of coal seam mining, the coal seam is damaged, and cracks appear due to the joint action of ground stress and machinery. Under the influence of pressure difference, gas diffuses to the mine through coal seam fissures and coal pores, which may lead to gas explosion, gas poisoning, gas suffocation, and other safety accidents [1–4]. For the prevention and control of coalbed methane in coal seam mining, coalbed methane pre-extraction is a common means. As a new type of coalbed methane pre-pumping tool, multi-branch plume drilling has attracted more and more attention [5]. The growing prevalence of

 doi:10.20944/preprints202604.1030.v1

multi-branch plume drilling has prompted significant research into the impact of drilling parameters on extraction efficiency [6–9]. Multi-branch pinnate boreholes have drawn increased attention in coal seam pre-extraction due to their feasibility in effectively extracting methane in low permeability coal seams. For the study of multi-branch plume drilling, numerous scholars have concentrated their attention on a number of key variables, including the diameter of the drill holes, the angle between the branch holes and the main drill holes, and the spacing and the length of the branch holes. However, there is considerable variation in the mathematical models and software employed in this research field [10–12].

Wang et al. established a heat–fluid–solid coupling model and applied it to the gas extraction simulation of bedding boreholes. They noted that with the progress of gas extraction, the temperature of the coal seam decreased around the borehole. This indicates that a large amount of gas desorption and migration near the borehole occurs. In addition, they carried out a model simulation without considering the temperature field and found that, in the same extraction time, when comparing the effect of reducing the pressure of coal seam gas, the effect of the model with an alteration in temperature is higher than that of the model without a change in temperature [13]. The model established by Zuo et al. in a study that injected N_2 to increase CH_4 production capacity took into account the stress model and the thermal model. A single bedding borehole was then used to simulate gas injection and gas extraction. The experiment revealed that the higher the initial temperature of the coal seam was, the smaller the thermal expansion and deformation of the coal seam skeleton and the less obvious the increase in the permeability of the coal seam. Higher temperatures can promote the desorption of adsorbed gas in coal seams and improve the recovery rate [14]. Ning et al. explored improvements in natural gas production by multi-branch wells by using the fluid–solid coupling model. They found that due to the existence of synergistic depressurization between branches and the increase in production intervals, branch wells can significantly improve the recovery of natural gas. Increasing the number of branches can further promote the synergistic effect and participation area. However, in a silty clay reservoir, this promotion effect decreases with the extension of the production cycle [15]. Wang et al. studied the Klinkenberg effect using the coal beam fire rod model. They found that the ratio of permeability alteration caused by the Klinkenberg effect was greater than that of the model without the Klinkenberg effect. If the Klinkenberg effect is not considered, the apparent permeability may be underestimated [16]. Wang et al. studied the influencing factors of coal seam permeability. They found that the slippage effect is affected by pore pressure and effective stress as well as temperature. Gas slippage has a significant impact on the permeability of rock. Due to the slippage effect, the apparent permeability of the coal is greater than the absolute permeability [17].

Through previous studies, it can be concluded that in the process of gas migration, it is meaningful to consider the variation in coal seam thermodynamics and the influence of the slippage effect. However, the majority of the models containing these factors are applied to simple borehole models. Taking a high-gas extra-thick coal seam as the research background, when considering the slippage effect and thermodynamic changes, the field of multi-branch plume drilling for gas extraction has not been optimized. Therefore, under the above background, this paper explores the influence of the angle between the branch and the main hole on the extraction effect and the influence of the branch length on the extraction effect. It provides a reference for improving the mathematical characterization model of coalbed methane flow. It lays a foundation for studying the parameters of multi-branch plume drilling.

2. Geological Conditions of the Coal Seams

The GJH coal mine is situated in the northern region of Linyou County, Shaanxi Province, China. The majority of the recoverable coal seam is the No. 3 coal seam. The top plate of the No. 3 coal seam is characterized by the presence of sandy mudstone, with an average thickness of approximately 1.00 m. Additionally, there is a layer of charcoal mudstone pseudo-topping, with a thickness ranging from 0.10 to 0.80 m. It is notable that individual sections are in direct contact with the sandstone at the base of the second section. The base plate is composed of carbonaceous mudstone, with a maximum

 doi:10.20944/preprints202604.1030.v1

thickness of 8.60 m (see Figure 1). The depth of the coal seam in the research working face lies in the range between 598 m and 665.5 m, with a temperature of 26.85 °C. The self-weight stress of the overlying strata on the coal seam is 7.858 MPa. The length of the coal seam in the working face is set at 2000 m, and the inclined length is designed to be 200 m. The average thickness of the coal seam is 8.5 m (see Table 1). The measurement results of the basic parameters of the coal seam gas indicate that the absolute CH_4 outflow of the working face is 15.56 m^3/min, which is characteristic of an especially thick high-gas coal seam that can be pumped out.

Table 1. Coal seam parameters.

Coal Seam Parameters	Numerical Value
Burial depth of coal seam	598 m~665.5 m
Geothermal temperature	26.85 °C
Pressure above coal seam	7.858 MPa
Coal seam length of working face	2000 m
Inclined length of working face coal seam	200 m
Average thickness of coal seam	8.5 m

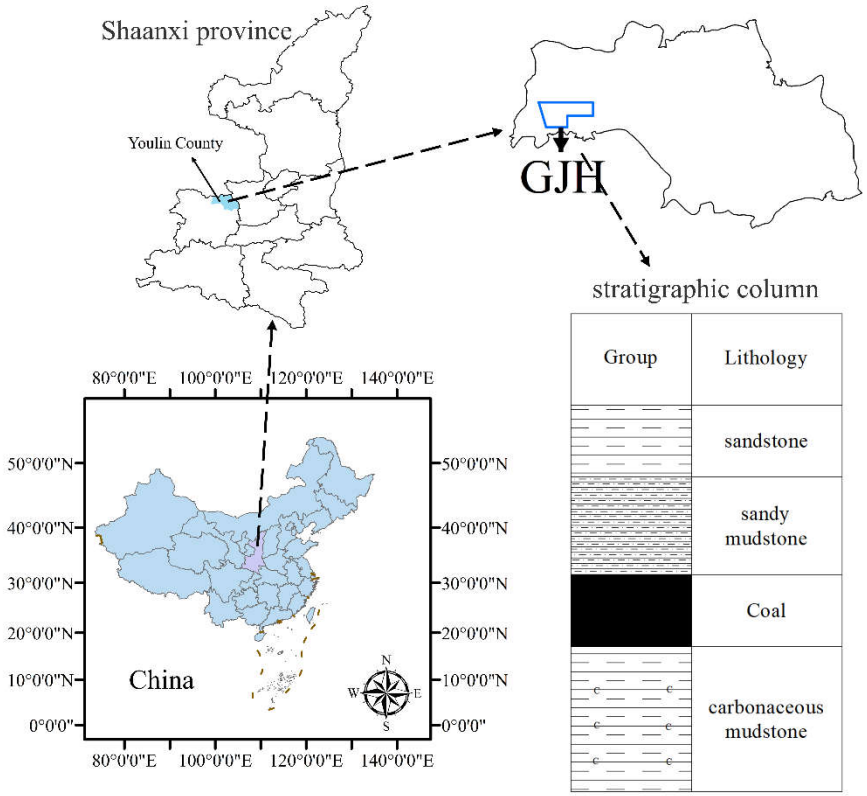

Figure 1. Geographic location map and stratigraphic histogram of the well field.

3. Mathematical Modeling

3.1. The Coal Matrix Gas Diffusion Equation

In the case of non-isothermal conditions and the absorption of CH_4 gas per unit mass of the coal body, the modified equation, Vs, is expressed as follows [18]:

$$V_s = \frac{V_L P_m}{P_m + P_L} \exp\left(-\frac{C_1(T - T_r)}{1 + C_2 P_m}\right) \quad (1)$$

where V_L is the Langmuir volume (m^3), P_L is the Langmuir pressure constant (MPa), P_m is the CBM gas pressure in the pores of the coal matrix (MPa), C_1 is the temperature coefficient in the non-

 doi:10.20944/preprints202604.1030.v1

isothermal adsorption process (1/K), C_2 is the pressure coefficient in the non-isothermal adsorption process (1/MPa), and T_r is the reference temperature of the adsorption measurement (K).

Subsequently, the mass per unit volume of the adsorbed gas within the matrix can be calculated [19]:

$$m_1 = \frac{V_L P_m}{P_m + P_L} \rho_a \rho_s \exp\left(-\frac{C_1(T - T_r)}{1 + C_2 P_m}\right) \tag{2}$$

where m_1 is the mass of adsorbed coal seam gas per unit volume of the coal pore system (kg/m³), ρ_s is the apparent density of coal (kg/m³), and ρ_a is the density of gas in standard conditions (kg/m³).

The density of the free coal seam gas within the matrix can be calculated as follows [20–22]:

$$\rho_m = \frac{M_c}{RT} P_m \tag{3}$$

where ρ_m is the density of free state coal seam gas (kg/m³), M_c is the molar mass of CH_4 gas (g/mol), and R is the molar constant of the gas (J/(mol·K)).

The mass per unit volume of free state coal seam gas is as follows:

$$m_2 = \varphi_m \rho_m = \varphi_m \frac{M_c}{RT} P_m \tag{4}$$

where m_2 is the mass of free state coal seam gas per unit volume of the coal pore system (kg/m³), and φ_m is the porosity of the coal matrix (%).

The adsorbed gas and the free gas collectively constitute the coal seam gas within the coal matrix. Consequently, the total mass of coal seam gas per unit volume of the coal matrix can be expressed as follows:

$$m_m = m_1 + m_2 = \frac{V_L P_m}{P_m + P_L} \rho_a \rho_s \exp\left(-\frac{C_1(T - T_r)}{1 + C_2 P_m}\right) + \varphi_m \frac{M_c}{RT} P_m \tag{5}$$

The free state coal seam gas continuously moves from the coal matrix to the coal seam fissure under the prompting of the concentration difference. This results in a large amount of free state gas being stored in the coal fissure, and the gas in the fissure also follows the ideal gas equation. Therefore, the density of free state coal seam gas in the fissure can be calculated as follows:

$$\rho_f = \frac{M_c}{RT} P_f \tag{6}$$

where P_f is the coal pore methane pressure (MPa).

The mass of free state CBM is

$$m_f = \varphi_f \rho_f = \varphi_f \frac{M_c}{RT} P_f \tag{7}$$

where φ_f is the fracture rate of the coal fissure (%).

The adsorbed state and free state coal seam gas within the coal matrix, along with the free state coal seam gas within the coal fissure, collectively constitute the coal seam gas within the coal body. The total mass of coal seam gas per unit volume of coal can be calculated by combining the results of Equations (5) and (7):

$$m = \frac{V_L P_m}{P_m + P_L} \rho_a \rho_s \exp\left(-\frac{C_1(T - T_r)}{1 + C_2 P_m}\right) + \varphi_m \frac{M_c}{RT} P_m + \varphi_f \frac{M_c}{RT} P_f \tag{8}$$

Given that the diffusion of coal seam gas is dependent on the concentration of the gas in question, it follows that the rate of gas exchange can be expressed as follows [23,24]:

$$Q_s = D\sigma_c (c_m - c_f) \tag{9}$$

where c_m is the concentration of CBM in the matrix pores (kg/m³), and c_f is the concentration of CBM in the fractures (kg/m³) and can be expressed as follows:

$$c_m = \frac{M_c P_m}{RT} \tag{10}$$

$$c_f = \frac{M_c P_f}{RT} \tag{11}$$

 doi:10.20944/preprints202604.1030.v1

where D is the diffusion coefficient of CH_4 gas (m^2/s). The diffusion coefficient of coal seam gas can quantitatively express the diffusion capacity of coal seam gas, which is affected by concentration, location, and time; the time-dependent exponential diffusion coefficient is as follows:

$$D = D_0 \exp(-\gamma t) \tag{12}$$

where D is the diffusion coefficient of the matrix at a certain moment (m^2/s), D_0 is the initial diffusion coefficient of the matrix (m^2/s), and γ is the attenuation coefficient of matrix diffusion coefficient (1/s).

σ_c is the shape factor of the cubic coal matrix, which can be expressed as follows [25]:

$$\sigma_c = \frac{3\pi^2}{L^2} \tag{13}$$

where L is the fissure distance (m).

Since the movement of gas follows the law of conservation of mass, the diffusion equation of coal seam gas movement from the matrix to the fissures is obtained by associating (5), (9), (10), (11), (12), and (13):

$$\frac{\partial m_m}{\partial t} = -D_0 \exp(-\gamma t) \frac{3\pi^2}{L^2} \frac{M_c}{RT} (P_m - P_f) \tag{14}$$

3.2. Gas Seepage Equation

Gas in the coal bed matrix is continuously diffused as a source of mass into the coal seam fissures, while the flow of coal seam gas in the coal fissures follows the law of conservation of mass [26–28]:

$$\frac{\partial}{\partial t}(\varphi_f \rho_f) + \nabla(\rho_f V) = Q_s (1 - \varphi_f) \tag{15}$$

where V is the gas seepage velocity in the fissure (m/s).

After considering the Klingberg effect of fluid flow in porous media, the seepage of coal seam gas in the cracks of coal seams following Darcy's law can be expressed as follows [29]:

$$V = -\frac{k_e}{\mu} \nabla P_f \tag{16}$$

where k_e is the effective gas permeability (m^2), which depends on the gas pressure, and μ is the dynamic viscosity (Pa·s).

The seepage equations of coal seam gas in the cracks of the coal seam are obtained by combining (6), (9), (10), (11), (13), (15), and (16):

$$\varphi_f \frac{\partial P_f}{\partial t} + P_f \frac{\partial \varphi_f}{\partial t} - \nabla\left(\frac{k_e}{\mu} P_f \nabla P_f\right) = D \frac{3\pi^2}{L^2} \frac{M_c}{RT} (1 - \varphi_f)(P_m - P_f) \tag{17}$$

3.3. Deformation Control Equation

Assuming that the coal body is a homogeneous, isotropic, elastic medium, under the condition of neglecting inertial forces, the stress balance equation is the following [30]:

$$\sigma_{ij,j} + F_i = 0 \tag{18}$$

where σ_{ij} is the stress tensor component and F_i the component of the volume force.

The coal body strain-displacement relationship is

$$\varepsilon_{ij} = \frac{1}{2}(u_{i,j} + u_{j,i}) \tag{19}$$

where ε_{ij} is the strain tensor component (dimensionless), and u is the deformation displacement (m).

Assuming that the coal seam is a double-pore medium consisting of pores and fissures and only the fissures have permeability, the effective law of the pore–fissure medium is the following [31]:

$$\sigma'_{ij} = \sigma_{ij} + (\beta_f P_f + \beta_m P_m)\sigma_{ij} \tag{20}$$

where σ_{ij}' is the effective stress (MPa), σ_{ij} is the total stress, $\beta_f = 1 - K/K_m$, $\beta_m = K/K_m - K/K_s$, $K = E/(3(1-2v))$, $K_s = K_m/[1 - 3\varphi_m(1-v)/(2(1-2v))]$, $K_m = E_m/3(1-2v)$, β_f is the effective stress coefficient of the cleavage and is dimensionless, β_m is the effective stress coefficient of the matrix and is dimensionless, K is the bulk

 doi:10.20944/preprints202604.1030.v1

modulus of the coal seam (MPa), K_s is the bulk modulus of the coal skeleton (MPa), K_m is the bulk modulus of the coal matrix (MPa), E is the modulus of elasticity of the coal seam (MPa), v is the Poisson ratio of the coal seam and is dimensionless, and E_m is the modulus of elasticity of the coal matrix (MPa).

In a three-dimensional state, the coal seam deformation follows the generalized Hooke's law:

$$\sigma'_{ij} = \lambda\delta_{ij}\varepsilon_v + 2G\varepsilon_{ij} \tag{21}$$

where $\lambda = 2G/(1-2v)$, $G = E/2(1+v)$, $\varepsilon_v = \varepsilon_{11} + \varepsilon_{22} + \varepsilon_{33}$;m$\varepsilon_{ij} = (u_{i,j} + u_{j,i})/2$, σ_{ij}' is the effective stress tensor (MPa), λ is the Mellar constant (MPa), δ_{ij} is the Kronecker symbol (dimensionless), G is the shear modulus of the coal seam (MPa), ε_v is the volumetric strain of the coal body (dimensionless), and ε_{ij} is the strain tensor (dimensionless).

Equations (18), (19), (20), and (21) are obtained by association:

$$Gu_{i,ij} + \frac{G}{1-2v}u_{j,ji} - \beta_f P_{f,i} - \beta_m P_{m,i} + F_i = 0 \tag{22}$$

The above and following equations are explained as follows: $E_{i,ij}$ is in tensor form and e can be displacement u, pressure P, and strain ε, where the first subscript denotes the component of the variable e in the i-direction, the second subscript denotes the partial derivatives of e_i in the i-direction, and the third subscript denotes the partial derivatives of $e_{i,I}$ in the j-direction; the subscripts I, $j = x$, y, z.

After considering the matrix adsorption/desorption and temperature-induced shrinkage deformation, the coal seam deformation control equation is obtained:

$$Gu_{i,jj} + \frac{G}{1-2v}u_{j,ji} - \beta_f P_{f,i} - \beta_m P_{m,i} - K\alpha_T T_{,i} + \left[\frac{KP_m}{P_m + P_L}\exp\left(-\frac{C_1(T-T_r)}{1+C_2P_m}\right)\right]_{,i} + F_i = 0 \tag{23}$$

3.4. Coal Seam Temperature Field Control Equations

Coal seam gas exchanges are heated by the coal reservoir in the fissures, which is usually regarded as a local thermal equilibrium, i.e., the fluid temperature is equal to the coal body temperature. According to the law of conservation of energy, the controlling equation for the temperature field of the porous medium is the following [32,33]:

$$\frac{\partial\left[\left(\rho c_p\right)_{eff}T\right]}{\partial t} + \rho_f c_{p,f} q\nabla T - \nabla\cdot\left(k_{eff}\nabla T\right) = -Q_E \tag{24}$$

where T is the temperature of the coal seam (K), $c_{p,f}$ is the heat capacity of the fluid (J/(Kg·K)), $(\rho c_p)_{eff}$ is the effective specific heat capacity of the coal body (J/(m³/K)), k_{eff} is the effective thermal conductivity (W/(m·K)), and Q_E is the heat transfer between the gas and the coal seam.

$(\rho c_p)_{eff}$ is the effective specific heat capacity of the coal body, which is expressed as follows:

$$\left(\rho c_p\right)_{eff} = (1-\varphi)\rho_s c_{p,s} + \varphi_f \rho c_{p,f} \tag{25}$$

and k_{eff} is the effective thermal conductivity, which is expressed as follows:

$$k_{eff} = (1-\varphi)k_s + \varphi_f k_f \tag{26}$$

where $c_{p,s}$ is the heat capacity of the coal seam (J/(Kg·K)), and k^s is the thermal conductivity of the coal seam (W/(m·K)).

The flow of gas in a coal seam is, to some extent, affected by the kinetic viscosity of the gas, which, according to Sutherland's law, changes by the temperature at which it is exposed. Therefore, the equation of variation in coal seam gas affected by temperature is as follows:

$$\mu = \mu_0\left(\frac{T_0 + C}{T + C}\right)\left(\frac{T}{T_0}\right)^{3/2} \tag{27}$$

where T_0 is the initial temperature of the coal seam (K), μ_0 is the initial kinetic viscosity of the gas (Pa·s), and C is Sutherland's constant (110.4K).

 doi:10.20944/preprints202604.1030.v1

3.5. Permeability Modeling

Under the consideration of effective stress variation, temperature variation, and coal matrix deformation, the coal matrix porosity is as follows [34]:

$$\varphi_{\mathrm{m}} = \frac{1}{(1+S)}(\varphi_{\mathrm{m0}}(1+S_0)+\alpha\ (S-S_0)) \tag{28}$$

$$\varphi_{\mathrm{m}} = \frac{1}{(1+S)}(\varphi_{\mathrm{m0}}(1+S_0)+\alpha\ (S-S_0)) \tag{29}$$

$$S_0 = \varepsilon_{\mathrm{v0}} + \frac{P_{\mathrm{m}}}{K_{\mathrm{s}}} - \varepsilon_{\mathrm{L}}\frac{P_{\mathrm{m0}}}{P_{\mathrm{m0}}+P_{\mathrm{L}}} - \alpha_T T_0 \tag{30}$$

where $\alpha = 1-K/K_s$, α is the Biot coefficient (dimensionless), φ_m is the coal matrix porosity (%), φ_{m0} is the initial coal matrix porosity (%), ε_{v0} is the initial coal volume strain (dimensionless), P_{m0} is the initial gas pressure of the coal matrix (MPa), α_T is the thermal expansion coefficient of the coal skeleton (1/K), S is the matrix porosity strain, and S_0 is the initial matrix porosity strain.

Assuming that permeability and porosity satisfy a cubic relationship, the permeability of the coal seam is as follows:

$$k_f = k_{f0}\left(\frac{1}{(1+S)}\left[(1+S_0)+\frac{\alpha(S-S_0)}{\varphi_{m0}}\right]\right)^3 \tag{31}$$

where k_{f0} is the initial permeability of coal (mD).

The slip effect is very obvious in the case of low rock permeability and low pressure, so it cannot be ignored when constructing the dynamic permeability equation. After considering the slip effect, the dynamic equation of permeability of a coal seam corrected by Klinkenberg's equation is as follows [35]:

$$k_{\mathrm{f}}^{\mathrm{e}} = k_{\mathrm{f}}(1+\frac{b_{\mathrm{kf}}}{P_{\mathrm{f}}}) \tag{32}$$

$$b_{kf} = \frac{D_{kf}\mu}{k_{\mathrm{f0}}} \tag{33}$$

$$D_{\mathrm{kf}} = \frac{4k_{\mathrm{f0}}}{2.81708\sqrt{\frac{k_{\mathrm{f0}}}{\varphi_{\mathrm{f}}}}}\sqrt{\frac{\pi RT}{2M_{\mathrm{c}}}} \tag{34}$$

where b_{kf} is the Klinkenberg coefficient of the matrix (Pa), and D_{kf} is the Knudsen diffusion coefficient in the fissure (m^2/s).

Associating (31), (32), (33), and (34) yields the dynamic equation for coal seam permeability:

$$\mathrm{k_f}^{\mathrm{e}} = k_{f0}\left(\frac{1}{(1+S)}\left[(1+S_0)+\frac{\alpha(S-S_0)}{\varphi_{m0}}\right]\right)^3 (1+\frac{4k_{\mathrm{f0}}}{2.81708\sqrt{\frac{k_{\mathrm{f0}}}{\varphi_{\mathrm{f}}}}k_{\mathrm{f0}}P_{\mathrm{f}}}\sqrt{\frac{\pi RT}{2M_{\mathrm{c}}}}\mu) \tag{35}$$

3.6. Model Solving Methods

Figure 2 illustrates the intricate physical field coupling relationship of the coal seam gas transport model. The process begins with the adsorption and desorption of gas within the coal seam matrix, followed by diffusion to the fissures for mass exchange within the fissures (7) and (8). Ultimately, seepage is completed in the fissures. The coupling relationship between the gas diffusion field, the gas seepage field, and the stress field is manifested in the porosity and permeability (1) and in the effective stress and adsorption deformation (2). The interdependence of the matrix diffusion field, fissure seepage field, and temperature field are manifested through the processes of heat transfer, convection, gas adsorption (5), gas desorption, and density (6). The coupling relationship between the stress field and the temperature field is expressed as strain energy, heat transfer, heat

 doi:10.20944/preprints202604.1030.v1

capacity (3), and thermal stress (4). The temperature change in the coal bed causes the expansion and contraction of the coal body, generating temperature stress and strain. This, in turn, affects the strain energy, influencing heat transfer and heat capacity.

From the aforementioned coupling relationships of the physical fields, it is evident that the model employed in this study integrates the thermal field, stress field, and diffusion–seepage field. Compared with the previous model, the physical field considered is more comprehensive. Moreover, the incorporation of dynamic viscosity variations and the consideration of slippage effects enhance the model's fidelity to the actual gas flow process, thereby rendering the simulation more realistic and accurate.

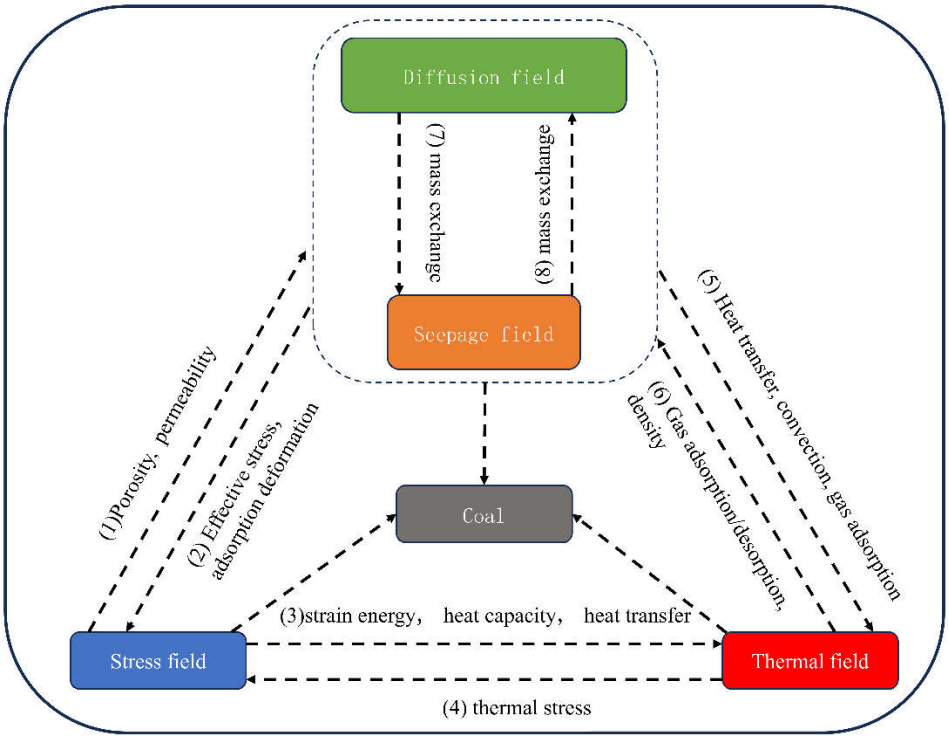

Figure 2. Multiphysics cross-coupling diagram.

4. Model Conditions and Validation Analysis

4.1. Modeling Study Conditions

In order to apply the coal seam gas flow THM coupled model to the engineering background, the COMSOL Multiphysics numerical software was used for testing. The following assumptions have been made:

1. The coal seam is regarded as a homogeneous and isotropic porous medium with dual pores and fissures. There is only fracture permeability in the coal seam. CH_4 gas exists in the pores and fissures. The flow of CH_4 gas satisfies the ideal state gas equation.
2. The mechanical deformation of the coal body is consistent with the linear elasticity assumption as well as the small deformation assumption. Furthermore, the strain in the coal matrix is regarded as infinitesimal.
3. Tensile stress is positive, whereas compressive stress is negative.
4. Without considering the influence of water in the coal seam, only the migration of CH_4 gas is considered. CH_4 gas diffuses into the fracture in the form of Fick's diffusion in the matrix. In the fracture, Darcy seepage migrates to the borehole. The adsorption and desorption of gas in the matrix meet the modified Langmuir equation.

In order to carry out the safe mining of coal seams, pre-mining extraction is conducted. The gas extraction rate is selected as 35%. The residual pressure of the coal seam should be 0.2535 MPa under

 doi:10.20944/preprints202604.1030.v1

the condition that the extraction rate is 35% and the original gas pressure is 0.6 MPa. When the coal seam gas pressure is less than or equal to 0.2535 MPa, it can be regarded as a safe area. A volume of coal seam gas pressure less than or equal to 0.2535 MPa is called the effective extraction volume. The parameters employed in the simulation experiment are presented in Table 2.

Table 2. Simulation parameters.

Notation	Parameter Name	Numeric	Unit
E	Modulus of elasticity of coal seam	2745	MPa
v	Poisson's ratio of coal seams	0.32	
k_0	Initial permeability of coal seam	4.82×10^{-16}	m^2
α_T	Coefficient of thermal expansion of coal skeleton	2.4×10^{-5}	1/K
$c_{p,s}$	Specific heat capacity of coal skeleton	1350	J/(kg·K)
k_{eff}	Effective thermal conductivity of coal skeleton	0.191	W/(m·K)
P_{m0}	Initial CH_4 pressure	0.6	MPa
V_L	Langmuir volume constant for CH_4	0.036	m^3/kg
P_L	Langmuir pressure constant for CH_4	3.034	MPa
ε_L	Langmuir strain constant for CH_4	0.0128	
u	Initial kinetic viscosity coefficient	1.84×10^{-5}	Pa·s
c	Sutherland's constant	110.4	K
C_1	Temperature coefficient of non-isothermal adsorption	0.023	1/K
C_2	Pressure coefficient for non-isothermal adsorption	0.072	1/MPa
D_0	Initial diffusion coefficient	5.42×10^{-12}	m^2/s
γ	Attenuation factor for matrix diffusion coefficient	2.72×10^{-12}	1/s
E_m	Modulus of elasticity of the matrix	8472	MPa
φ_{m0}	Initial porosity of matrix	9.58	%
F_Z	Coal seam overburden stress	−5	MPa
Φ_{f0}	Initial fracture ratio of the fissure	3.7	%

4.2. Model Validation

In order to verify the reliability of the mathematical model, the simulated gas production rate and actual gas production rate were applied. The model was established as shown in Figure 3. The geometric model of the coal seam is defined by a length of 2465 m, a width of 200 m, and a height of 8.5 m. The diameter of the borehole is 108 mm, and the length is 106 m. The upper boundary of the geometric model exhibits a pressure of 7.858 MPa. The smooth boundary is situated around the periphery. The fixed boundary is located at the bottom. The origin of the coordinates is situated in the lower left corner of the coal seam. A single borehole is located in the center of the coal seam thickness. The coordinate position of the borehole is (1232.5, 0, 4.25). The open end of the borehole is connected to the atmosphere. The internal boundary pressure of the borehole is 16 Kpa, representing the negative pressure of extraction. In the diffusion field and seepage field, the boundary of the model represents a condition of no flow and zero flow, respectively. In the temperature field, the boundaries of the model indicate thermally insulated conditions. The initial pore pressure of the model is 0.6 MPa, and the initial temperature of the coal seam is 305.5 K.

 doi:10.20944/preprints202604.1030.v1

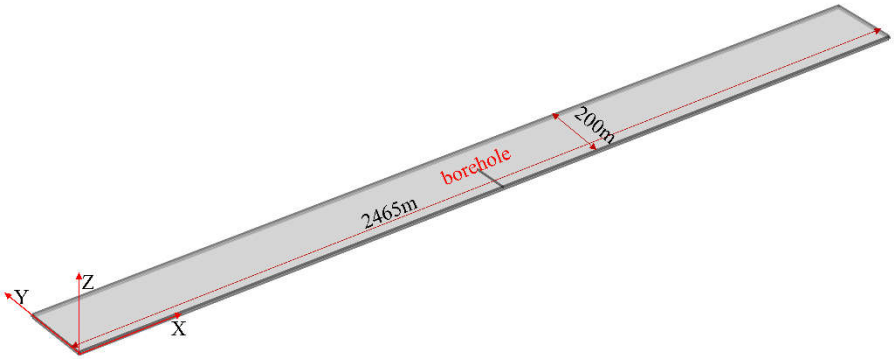

Figure 3. Diagram of the validated geometric model.

The experiment carried out a 360-day simulation of single-hole coal seam gas extraction. The gas production rate of the single-hole drainage coal seam was obtained by the simulation experiment and the fitting of the field single-hole production data (see Figure 4). It can be seen that the simulated production rate is basically consistent with the field measurements. In the early stages of extraction, the production rate decreased rapidly, and then the decline rate slowed down. This shows that a large amount of coal seam gas is quickly extracted in the early stages of extraction, and then the speed gradually slows down. This finding corroborates the reliability of the THM coupling model of coal seam gas transport.

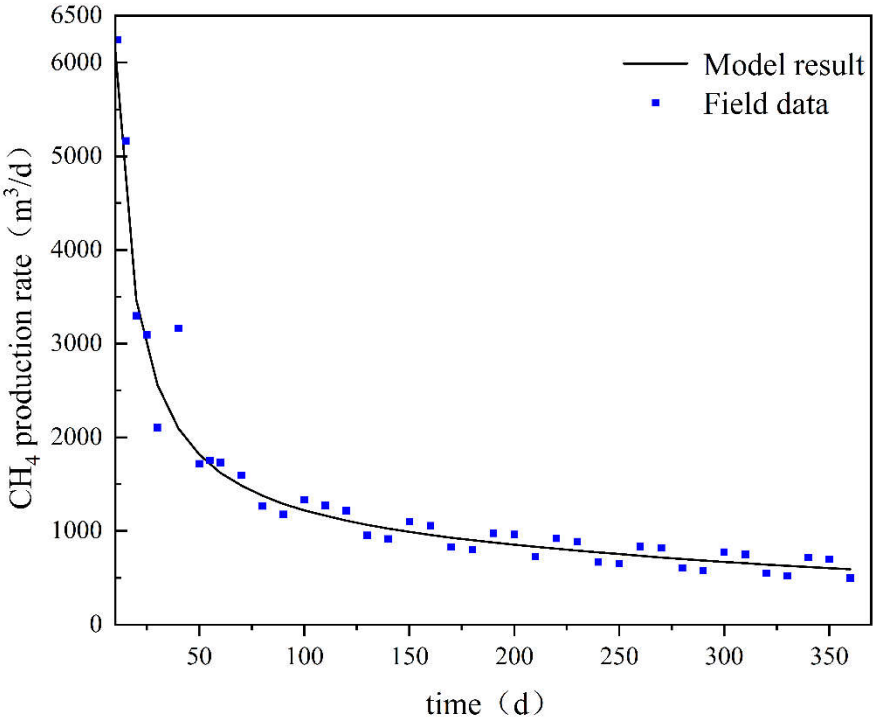

Figure 4. Fitted CH_4 production rate from the field data and numerical simulation.

4.3. Geometric Modeling of Multi-Branched Plume Boreholes

According to the original coal seam conditions and engineering equipment conditions, the geometric model is established (see Figure 5). The model is 400 m long, 200 m wide, and 8.5 m high. Other parameters are shown in Table 1. The boundary conditions are the same as before. The length of the main borehole was fixed at 400 m, while the angle of the branch borehole and the length of the branch borehole were modified. This design has the advantage of avoiding the interference of the positive and negative effects on the study due to changes in the main borehole.

 doi:10.20944/preprints202604.1030.v1

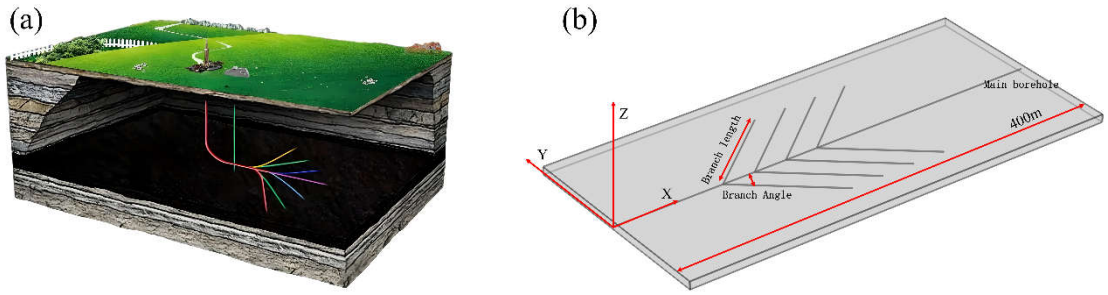

Figure 5. Geometrical modeling of multi-branching plume boreholes. (**a**) Real extraction profile. (**b**) Coal seam geometric model diagram.

5. Results

5.1. Branch Borehole and Main Borehole Clamping Angle Influence

In the experiment, the diameter of the drill hole was 113 mm, the spacing of the branch openings was 60 m, and the length of the branch was 100 m. The angles between the branch borehole and the main borehole were 30°, 40°, 50°, and 60°. The same experimental conditions were used to simulate gas extraction for 550 days.

Figure 6 illustrates the variation in average coal seam gas pressure in response to alterations in extraction time. During the initial 100 days of extraction, the difference in the average coal seam gas pressure at each angle is not significant. Within a certain angle range, the increase in angle results in a greater effect of coal seam gas pressure reduction, although the magnitude of the increase is decreasing. After exceeding the angle threshold, the pressure reduction effect begins to increase once more. As illustrated in Figure 6, the corresponding extraction control ranges for the 30° branch-to-main-hole angle and the 60° branch-to-main-hole angle at 450 days of extraction are presented.

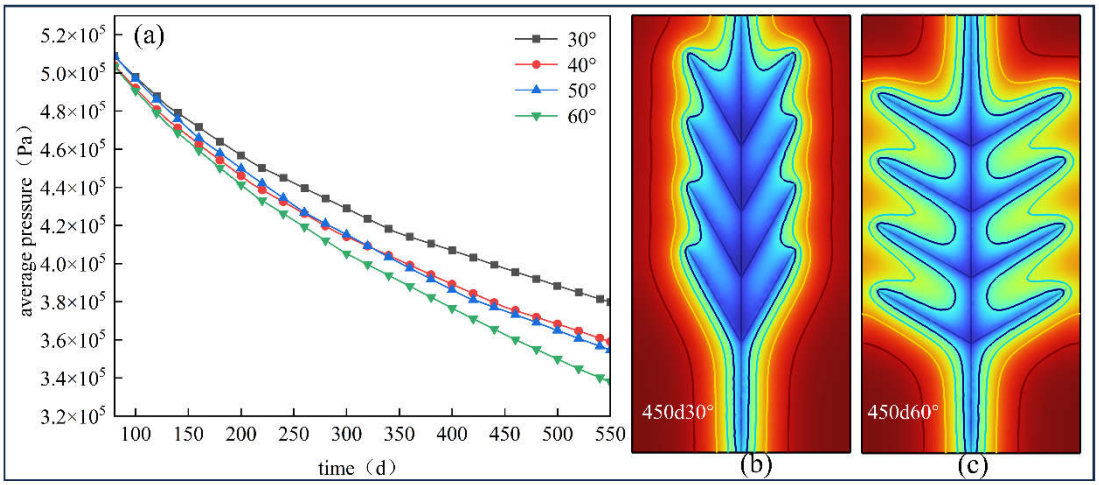

Figure 6. Variations in average coal seam gas pressure and pressure clouds. (**a**) Variations in the average coal seam gas pressure. (**b**) Coal seam pressure cloud diagram for a 30° branch angle. (**c**) Coal seam pressure cloud diagram for a 60° branch angle.

Figure 7 shows the changes in cumulative gas production and cumulative gas production per meter. The extraction time is 450 days. Under the conditions of 60°, 50°, 40°, and 30°, the growth rate of the former is 5.34%, 0.03%, and 9.82%, respectively, compared with the latter. It can be observed that as the angle between the branch borehole and the main borehole increases, the cumulative gas production demonstrates an increase. Within a specific angle range, the rise in gas production

 doi:10.20944/preprints202604.1030.v1

diminishes as the angle grows, subsequently exhibiting an increase after surpassing this critical angle. The cumulative gas production per meter exhibits a parallel trend.

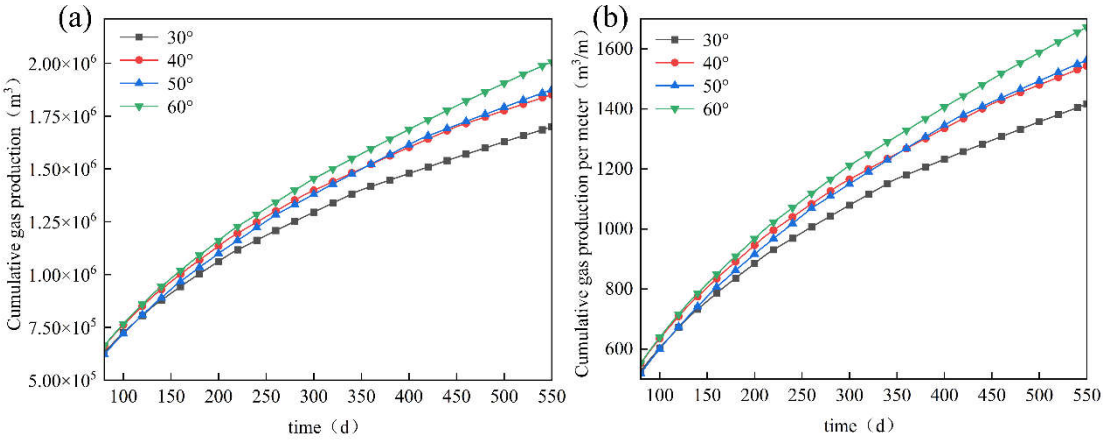

Figure 7. Cumulative gas production and cumulative gas production per meter. (**a**) Cumulative gas production. (**b**) Cumulative gas production per meter.

Figure 8 presents the variation in daily gas production with time. Within a certain angle range, with the increase in the angle between the branch borehole and the main borehole, the daily gas production increases, but the increase is decreasing. However, beyond a certain angular threshold, the magnitude of the increase in daily gas production begins to diminish.

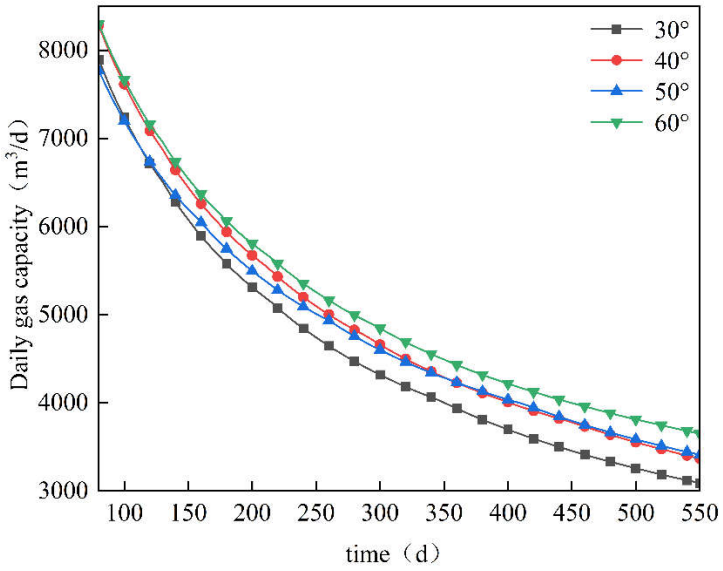

Figure 8. Daily gas production over time.

5.2. Branch Length Effects

In the experiment, the diameter of the borehole was 113 mm, the spacing of the branch holes was 60 m, and the angle of the main branch was 40°. The lengths of the branch boreholes were 50 m, 75 m, 100 m, and 125 m. The same experimental conditions were used to simulate the gas extraction for 550 days.

Figure 9 demonstrates the variation in the average coal seam gas pressure with the extraction time under different branch length schemes. As the extraction time increases, the average pressure of the coal seam gas demonstrates a trend of an initial rapid decline, followed by a slower reduction. At the outset of the extraction period, as the length of the branch borehole increases, the average pressure

 doi:10.20944/preprints202604.1030.v1

drop exhibits a considerable degree of variability. At 160 days of extraction, the gas pressure of the coal seam decreases by 14.385%, 18.438%, 19.893%, and 26.922% under the condition of a branch length of 50 m, 75 m, 100 m, and 125 m, respectively. It can be seen that in the early stages of extraction, an increase in branch length can better reduce the gas pressure of the coal seam. This shows that with the increase in extraction time, the gap between the decrease in the coal seam gas pressure caused by the increase in branch length gradually increases.

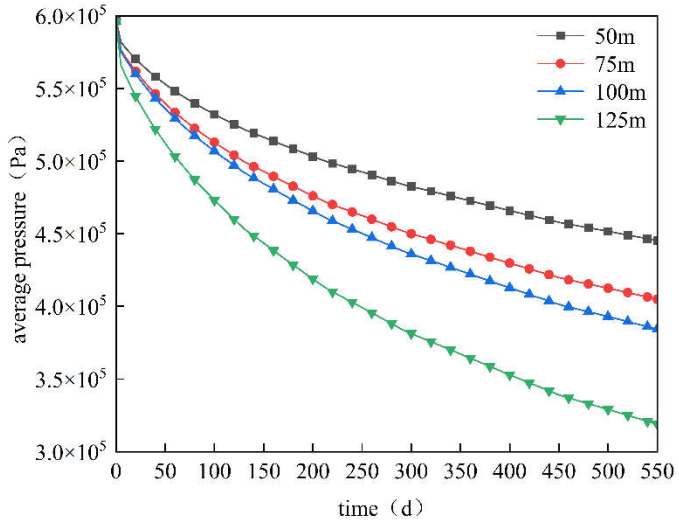

Figure 9. Variation in average coal seam gas pressure with extraction time.

Figure 10 illustrates the variation in cumulative and daily gas production with extraction time. The phenomenon of cumulative gas production with increasing branch length is indicative of the change in coal seam gas pressure. The daily gas production shows a large gap in the early stages of extraction, which reflects that the influence of branch length on the extraction range is very obvious. In the early stages of extraction, the longer the branch length is, the greater the quantity of coal seam gas pumped out.

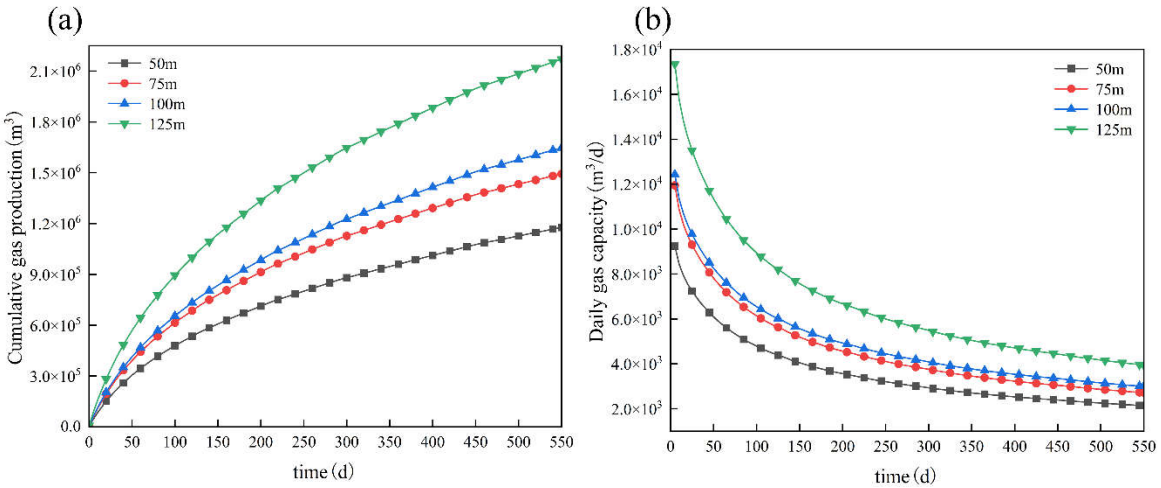

Figure 10. Cumulative gas production and daily gas production versus pumping time. (**a**) Cumulative gas production. (**b**) Daily gas production versus pumping time.

 doi:10.20944/preprints202604.1030.v1

6. Discussion

6.1. The Thermodynamic Effect

In the process of gas extraction, gas desorption is an endothermic process, which leads to a variation in coal temperature. The variation in temperature affects the deformation of the coal body and then affects the alteration in pore structure. In addition, the dynamic viscosity of the gas is affected by temperature alterations. In order to identify its role in the model, a geometric coal seam was established with a length of 400 m, a width of 200 m, and a height of 8.5 m. The borehole in the coal seam was 400 m long and 113 mm in diameter. The other experimental conditions were the same as those for previous experiments. At the same time, the monitoring line (x = 100, y ∈ (−100~100), Z = 0) was selected as shown in Figure 11.

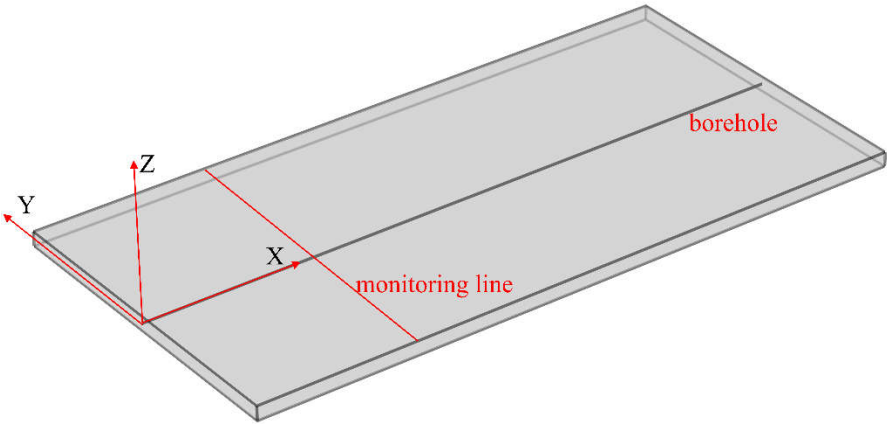

Figure 11. Coal seam geometry.

The simulated gas extraction was carried out for 550 days, and the temperature fluctuation of the coal seam on the monitoring line was obtained for 200 days, as shown in Figure 12. After gas extraction, the temperature of the coal seam was the shape of a funnel with the borehole at the center. The sharp drop in coal seam temperature near the borehole formed a rapid temperature drop zone. In this area, a large amount of gas was quickly removed near the borehole, and a large amount of gas molecules attached to the coal seam were desorbed. A severe endothermic reaction occurred inside the coal seam, and the temperature of the coal seam showed a rapid downward trend. The downward trend started from 27 m around the borehole. In the area about 27 m away from the borehole, the drilling control ability became extremely weak. The gas flow in the area was very slow, and the temperature of the coal seam did not change much.

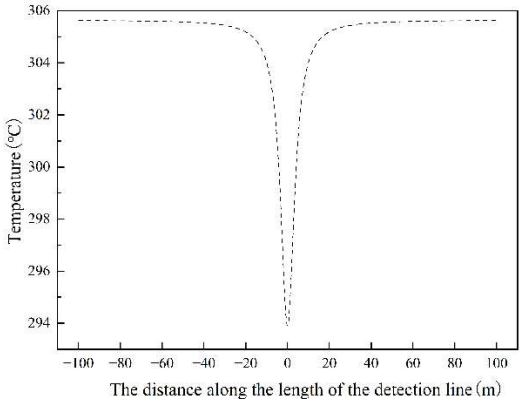

Figure 12. A 200-day monitoring line for coal seam temperature variation. (Monitor the temperature change of coal seam on line).

 doi:10.20944/preprints202604.1030.v1

Figure 13 shows the variation in the gas dynamic viscosity and the gas flow rate on the monitoring line when the extraction period is 200 days. When pumping for 200 days, the alteration in gas dynamic viscosity and the alteration in coal seam temperature show the same trend. The dynamic viscosity near the borehole decreases rapidly from the distance to the center of the borehole. However, there is almost no obvious fluctuation after 27 m from the borehole. This also verifies that gas dynamic viscosity is affected by temperature, as in Equation (27).

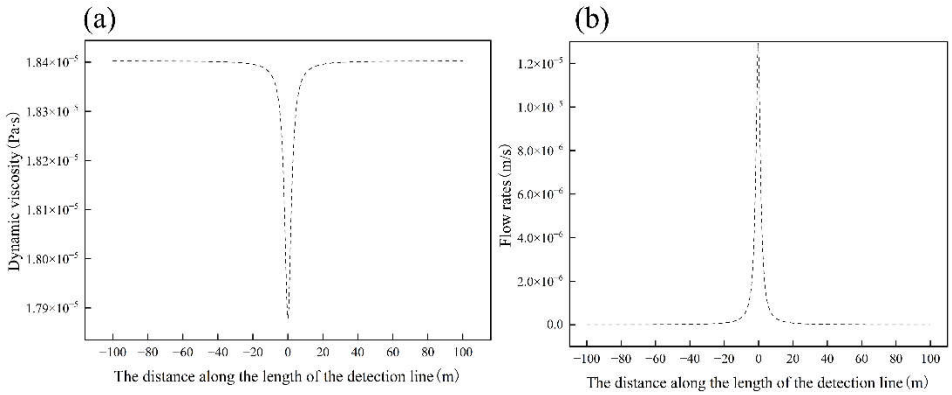

Figure 13. A 200-day monitoring line for gas dynamic viscosity and velocity alterations. (**a**) Dynamic viscosity. (The black line indicates the dynamic viscosity change on the monitoring line) (**b**) Flow rates. (The black lines indicate changes in the flow rate on the monitoring line).

The flow velocity of the gas is in the shape of a tower tip near the borehole, and the end point is about 27 m around the borehole. The closer the gas flow rate is to the borehole, the faster the growth is. The closer to the edge of the coal seam, the slower the flow rate is. The coal seam is divided into a fast flow zone and a slow flow zone. This phenomenon corresponds to the change in gas dynamic viscosity. The decrease in coal seam temperature makes the gas dynamic viscosity decrease, and the decrease in gas dynamic viscosity makes the coal seam gas flow quickly. It can be seen that the addition of a coal seam temperature field is necessary in the construction of a coal seam gas migration model.

6.2. The Slippage Effect

The slippage effect plays an important role in the study of gas seepage in low permeability porous media. Gas does not produce an adsorption thin layer at the inner wall of the porous medium, and the flow rate of the gas molecule is not significantly different from the flow rate at the fracture center and the fracture wall. This phenomenon becomes a gas slippage effect. The existence of the slippage effect greatly affects the process of fluid flow in porous media. The slippage effect can effectively reduce the friction between the gas and the inner wall of the porous medium, making the gas permeability larger.

In order to show the role of the slippage effect in the construction of a gas migration model, based on the experimental conditions established in the previous section, a model with a slippage effect and a model without a slippage effect were used for experiments. The simulation experiment obtained the coal seam gas pressure and permeability change in the monitoring line at 200 days, as shown in Figure 14. The coal seam gas pressure with a slippage effect is lower than that without a slippage effect. At the same distance of 16 m from the borehole, the pressure reduction effect with a slippage effect is 26.28% higher than that without a slippage effect. Similarly, the permeability around the borehole in the figure is higher, and the edge direction of the coal seam is lower. At 8 m away from the borehole, permeability with a slippage effect is 2.34% higher than that without a slippage effect. The increased permeability after considering the slippage effect makes the coal seam gas flow faster. At the same time, more coal seam gas is extracted, and the coal seam pressure with the slippage effect is smaller, which also illustrates this point.

 doi:10.20944/preprints202604.1030.v1

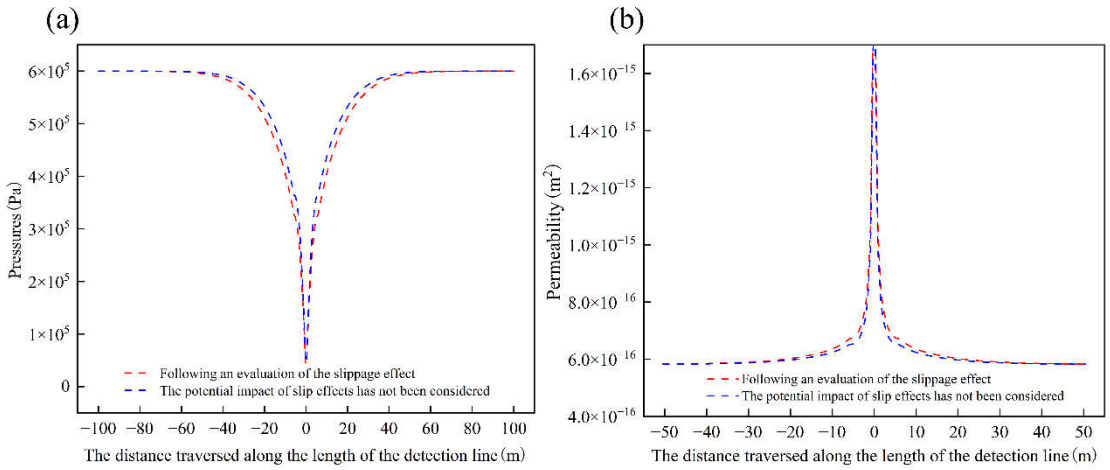

Figure 14. The changes in coal seam gas pressure and permeability on the monitoring line for 200 days. (**a**) Coal seam gas pressure. (**b**) Permeability.

6.3. The Borehole Angle Effect

The experimental results show that the gas production is the smallest under the condition of a 30° main branch angle. This is because the boreholes are relatively compact at this time, and the boreholes can quickly form a fully synergistic pressure drop zone and extend to the edge of the borehole. The increase in extraction time only makes the pressure drop shape formed by the borehole slowly increase along the outer contour, and the overall controllable range of the borehole is small. Therefore, gas production is not as good as at the other three angles. The extraction range controlled by the drilling structure at 40° and 50° angles is improved. At 460 days, it increased by 9.89% compared with the 30° angle structure. However, the overall controllable range of boreholes is still limited. Therefore, the difference is not large and is less than at the 60° angle.

For further analysis, the line (x = 130, y ∈ (-100 ~ 100), z = 0) was selected as the monitoring line. With the increase in extraction time, the change in the coal seam gas pressure on the line is shown in Figure 15. The gas pressure on the red line in the figure is 0.2535 MPa. The regional gas pressure under the red line is lower than 0.2535 MPa; that is, the target pressure for extraction is reached.

It takes 60% more time to obtain a branch angle of 40° than a branch angle of 30°. A branch angle of 50° takes 55% more time than a branch angle of 40°. It takes 45% more time when the branch angle is 60° than when the branch angle is 50°. This shows that with the increase in the angle between the branch borehole and the main borehole, the time required to form a complete synergy between the boreholes gradually increases, and the magnitude of this increase shows a decrease.

With the increase in the angle between the branch and the main hole, the distance between the boreholes becomes larger. When the extraction time is 100 days, the controllable distances around the boreholes on the monitoring line at each angle are 3.9746 m, 2.6383 m, 2.6026 m, and 2.2958 m, respectively. The controllable drilling distance decreases gradually. This indicates that the increase in angle weakens the synergistic extraction effect between boreholes. It is more and more difficult to form the overlap of the extraction range that can be affected by the drilling. Overlapping areas will gradually form with the passage of time. The coal seam gas pressure cloud diagram in Figure 16 also shows this phenomenon when the monitoring line forms a safety synergy.

 doi:10.20944/preprints202604.1030.v1

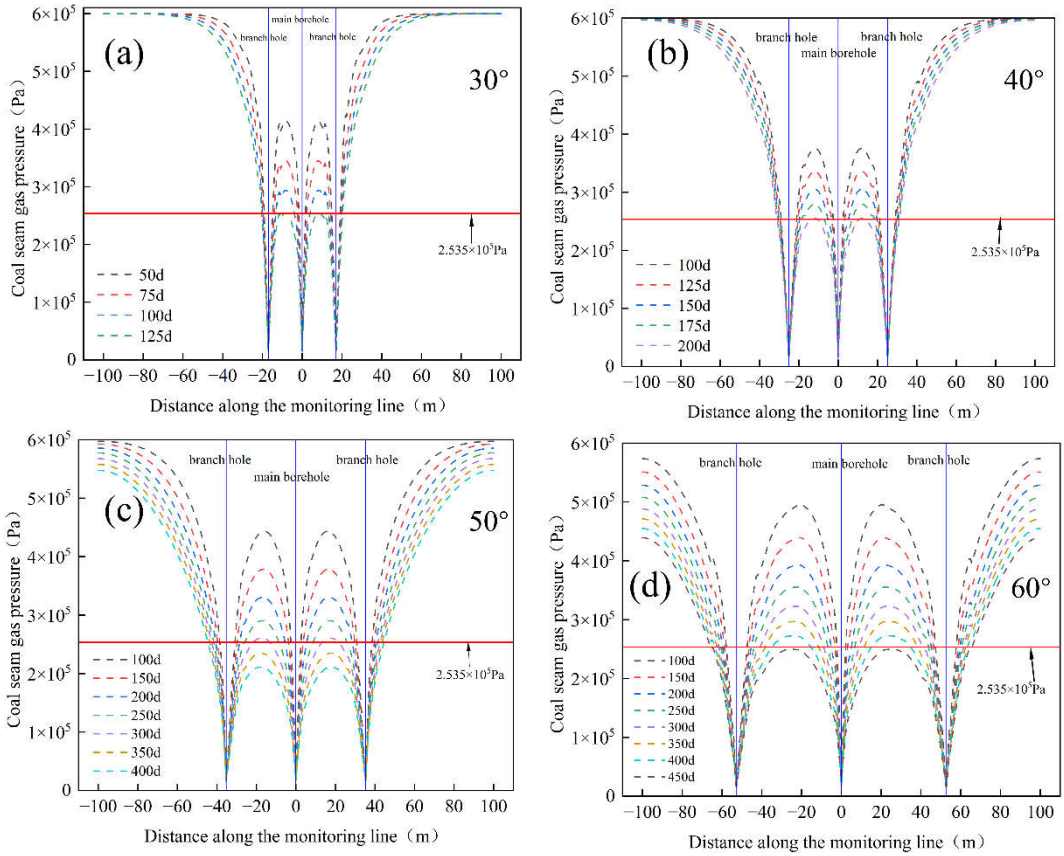

Figure 15. Variation in gas pressure in a coal seam at a monitoring line at various angles. (**a**) The change in gas pressure with a 30° branch angle. (**b**) The change in gas pressure with a 40° branch angle. (**c**) The change in gas pressure with a 50° branch angle. (**d**) The change in gas pressure with a 60° branch angle.

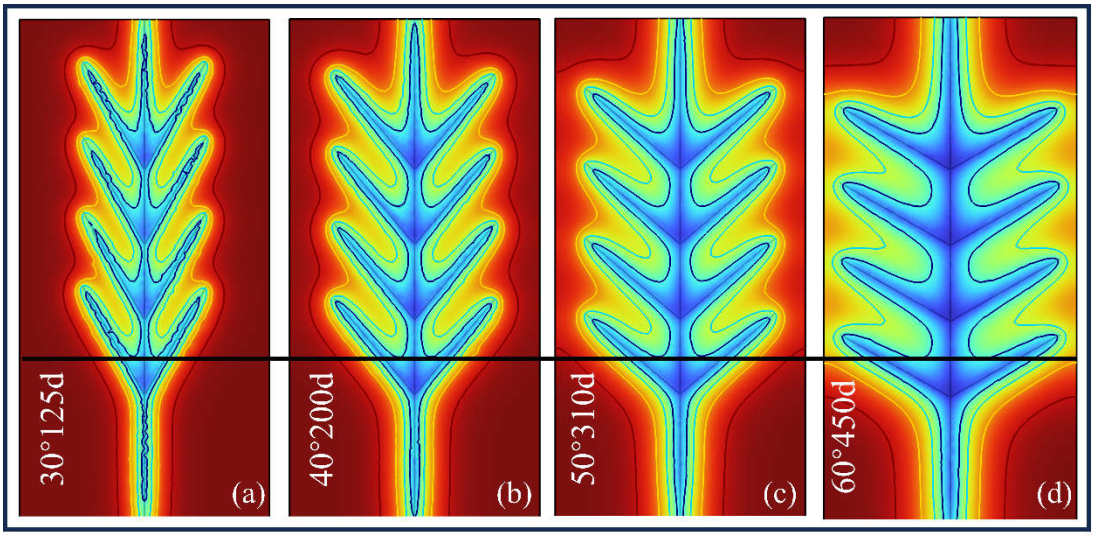

Figure 16. Coal seam gas pressure cloud when extraction is fully synergized. (**a**) Coal seam pressure cloud diagram with a 30° branch angle. (**b**) Coal seam pressure cloud diagram with a 40° branch angle. (**c**) Coal seam pressure cloud diagram with a 50° branch angle. (**d**) Coal seam pressure cloud diagram with a 60° branch angle.

6.4. The Branch Length Effect

When the branch length is small, the synergistic depressurization effect between boreholes cannot be fully utilized. An increase in branch length can improve the effect of synergistic depressurization, and the controllable range of the extraction boreholes gradually increases. When

 doi:10.20944/preprints202604.1030.v1

the branch length is within a critical value, the effect of continuing to increase the branch length gradually decreases. The effective synergistic pressure drop zone is only continuously expanding at a weak speed according to the contour, so the increase in the reduction in coal seam gas pressure is not as good as before. After exceeding this critical length, the branch borehole gradually approaches the edge of the coal seam. The overall control range of drilling is obviously larger, and the effect of gas extraction from the coal seam is significantly increased.

Figure 17 presents the variation in effective extraction volume with extraction time and the gas pressure cloud diagram of the coal seam at 550 days of extraction. When the length of the branch hole is below 100 m, the effective volume increases with the increase in the branch length. The amplitude of the increase is decreasing, which also explains the alteration trend in the coal seam pressure and gas production. The branch length increases from more than 100 m to 125 m, making the borehole closer to the edge of the coal seam. The range that the whole borehole can control has been greatly improved. The extraction effect on coal seam gas has also been greatly enhanced.

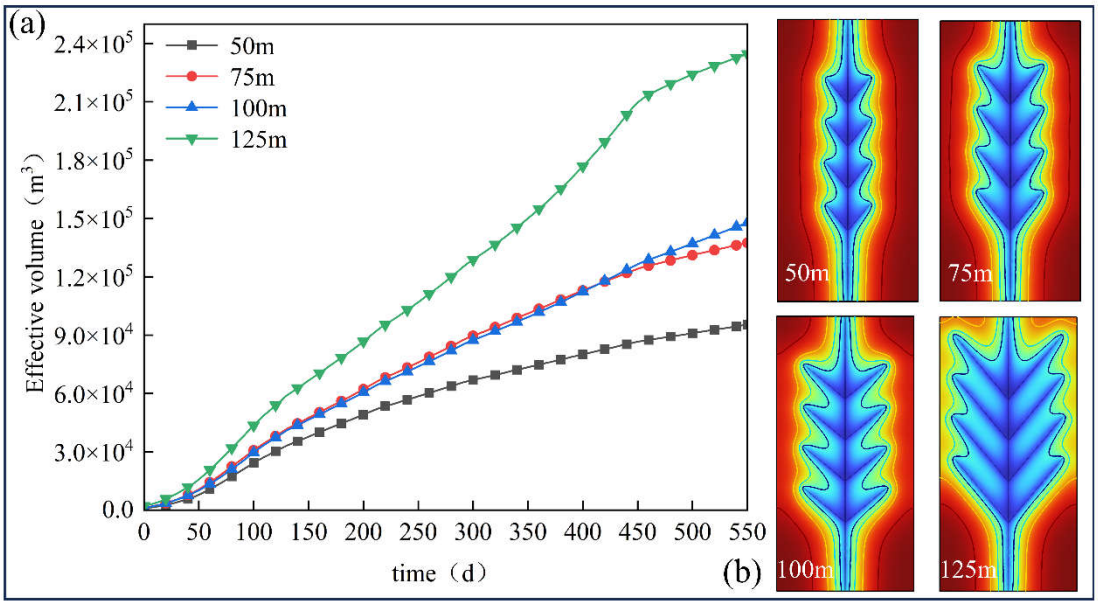

Figure 17. Effective volume change with time and gas pressure distribution cloud map. (**a**) Effective volume. (**b**) Gas pressure cloud diagram of a coal seam for each branch length over 550 days.

7. Conclusions

This paper takes the high-gas extra-thick coal seam as the research background. A CBM migration model including the diffusion field, seepage field, stress field, and temperature field is established. At the same time, the influence of the slippage effect on the dynamic permeability equation and temperature on gas dynamic viscosity are considered. Based on this, the influence exerted by the branch length and the angle of branch divergence on the drainage effect was investigated, and the main conclusions are as follows:

1. The coal seam temperature changes with the progress of coal seam gas extraction, and the coal seam temperature near the borehole decreases. The decrease in the coal seam temperature reduces the gas dynamic viscosity. The decrease in dynamic viscosity increases the gas flow rate. It is necessary to add thermodynamics to the mathematical model. The slippage effect can increase permeability, and the simulation results for dynamic permeability without considering the slippage effect are different.
2. The angle between the branch borehole and the main borehole has a strong influence on the extraction effect. Within a certain range, the increase in branch angle can expand the control range of drilling. The synergistic depressurization effect between boreholes is fully utilized, and the gas extraction effect is promoted. However, as the angle continues to increase, the

 doi:10.20944/preprints202604.1030.v1

improvement in extraction effect is weakened. The time to obtain a better extraction effect also increases. The increase in the angle makes the branch move closer to the edge of the coal seam, and the expansion of the overall control range of the borehole makes the extraction effect better.

3. The influence of branch length on the extraction effect is very obvious. The increase in branch length can greatly improve the range of drilling control and the extraction effect. When the branch length increases to a certain range, the increase in the branch length gradually weakens the improvement of the extraction effect. When the branch length exceeds this critical value and approaches the edge of the coal seam, the expansion in the overall control range of the borehole makes the extraction effect better. However, the selection of drilling length should be combined with cost, opening difficulty, extraction time, and other aspects.

Author Contributions: For research articles with several authors, a short paragraph specifying their individual contributions must be provided. The following statements should be used "Conceptualization, Q.Z.; methodology, Q.Z.; software, Z.Q.; writing—original draft preparation, Q.Z.; writing—review and editing, Q.Z.; visualization, Q.W.; supervision, J.J.; project administration, J.J.; funding acquisition, J.J.

Funding: This research was supported by the Knowledge Innovation Program of Wuhan-Shuguang Project (No. 2022010801020360) and the Hubei Province technology innovation plan key research and development projects (No. 2023BCB084). We are grateful to anonymous reviewers for their valuable comments on the manuscript.

Data Availability Statement: The data presented in this study are available on request from the corresponding author due to (specify the reason for the restriction).

Conflicts of Interest: The authors declare that they have no known competing financial interests or personal relationships that could have appeared to influence the work reported in this paper.

Nomenclature

E	Elastic modulus of the coal seam (MPa)
V	Poisson's coal seam ratio
k_0	Initial permeability of the coal seam (m^2)
α_T	Thermal expansion coefficient of the coal skeleton (1/K)
$c_{p,s}$	Specific heat capacity of the coal skeleton (J/(kg·K))
k_{eff}	Effective thermal conductivity of the coal skeleton (W/(m·K))
P_{m0}	Initial CH_4 pressure (MPa)
V_L	Langmuir volume constant of CH_4 (m^3/kg)
P_L	Langmuir pressure constant of CH_4 (MPa)
ε_L	Langmuir strain constant of CH_4
u	Initial kinetic viscosity coefficient (Pa·s)
c	The Sutherland constant (K)
C_1	Temperature coefficient of non-isothermal adsorption (1/K)
C_2	Pressure coefficient of non-isothermal adsorption (1/MPa)
D_0	Initial diffusion coefficient (m^2/s)
γ	Attenuation coefficient of the matrix diffusion coefficient (1/s)
F_Z	The elastic modulus of the matrix (MPa)
Φ_{f0}	The initial fracture rate of the fracture (%)

References

1. Zhang, C.; Qian, X. Design of gas control lane of 9# coal seam in Wuhushan Mine based on layer layout optimization. *Sci. Rep.* **2024**, *14*, 22520.
2. Zhao, C.; Gao, P.; Ruan, J.; Pu, Y.; Sun, Y.; Cheng, X.; Sun, Y. Research on Hotspots and Evolutionary Trends in Coal Mine Gas Prevention. *Processes* **2024**, *12*, 1993.
3. Gao, H.; Gao, Y.; Qi, J.; Fu, Q.; Zhang, X. Study on surrounding rock deformation and gas control of entry automatically formed by roof cutting in high-gas coal seam. *Energy Explor. Exploit.* **2023**, *41*, 1559–1575.
4. He, L.; Dai, Y.; Xue, S.; Zheng, C.; Han, B.; Guo, X. Study on gas control methods optimization for mining safety. *Adv. Civ. Eng.* **2021**, *2021*, 4594330.

 doi:10.20944/preprints202604.1030.v1

5. Li, Q.; Li, Q.; Wu, J.; Li, X.; Li, H.; Cheng, Y. Wellhead Stability during Development Process of Hydrate Reservoir in the Northern South China Sea: Evolution and Mechanism. *Processes* **2024**, *13*, 40.
6. Zhang, D.; Zhang, M.; Wang, L.; Zeng, R.; Wang, J. Determination and application of reasonable levels for highly directional long boreholes in deep outburst coal seams. *Geofluids* **2022**, *2022*, 3621921.
7. Guo, T.; Wang, W.; Yang, X.; Chen, M.; Xu, H.; Guan, L.; Lv, M. Numerical simulation of gravel packing in multi-branch horizontal wells in hydrate reservoirs based on CFD-DEM coupling. *Geoenergy Sci. Eng.* **2025**, *244*, 213445.
8. Ma, T.; Chu, H.; Li, J.; Zhang, J.; Gao, Y.; Zhu, W.; John Lee, W. Rate transient analysis for multilateral horizontal well in natural gas hydrate: Superposition principle and reciprocity. *Int. J. Coal Sci. Technol.* **2024**, *11*, 70.
9. He, J.; Zhang, Y.; Luo, E.; Xu, A.; Chen, Y.; Liu, Y.; Zeng, X.; Jiang, L. A Coupling Model of Gas–Water Two-Phase Productivity for Multilateral Horizontal Wells in a Multilayer Gas Reservoir. *Processes* **2024**, *12*, 1643.
10. Enab, K.; Lopez, I.; Elmasry, Y. Synergizing shale enhanced oil recovery and carbon sequestration: A novel approach with dual lateral horizontal wells. *Int. J. Greenh. Gas Control.* **2024**, *135*, 104155.
11. Ye, H.; Chen, D.; Yao, Y.; Wu, X.; Li, D.; Zi, M. Exploration of production capacity-geomechanical evaluation and CO2 reinjection repair strategy in natural gas hydrate production by multilateral horizontal wells. *Energy* **2024**, *296*, 131097.
12. Jin, G.; Su, Z.; Zhai, H.; Feng, C.; Liu, J.; Peng, Y.; Liu, L. Enhancement of gas production from hydrate reservoir using a novel deployment of multilateral horizontal well. *Energy* **2023**, *270*, 126867.
13. Wang, K.; Wang, Y.; Xu, C.; Xu, Z.; Guo, H.; Liu, Y.; Dong, H. Transition of dominated factors in coal seam gas migration: Thermo-hydro-mechanical modeling and analysis. *Int. J. Heat Mass Transf.* **2025**, *236*, 126239.
14. Zuo, W.; Li, L.; Liu, Y.; Han, H.; Cui, P. Modeling Study of Enhanced Coal Seam Gas Extraction via N2 Injection Under Thermal–Hydraulic–Mechanical Interactions. *ACS Omega* **2024**, *9*, 39051–39064.
15. Ning, F.; Chen, Q.; Sun, J.; Wu, X.; Cui, G.; Mao, P.; Li, Y.; Liu, T.; Jiang, G.; Wu, N. Enhanced gas production of silty clay hydrate reservoirs using multilateral wells and reservoir reformation techniques: Numerical simulations. *Energy* **2022**, *254*, 124220.
16. Wang, G.; Ren, T.; Wang, K.; Zhou, A. Improved apparent permeability models of gas flow in coal with Klinkenberg effect. *Fuel* **2014**, *128*, 53–61.
17. Wang, B.; Jing, H.; Zhang, Y.; Liu, X.; Tu, Q.; Song, X.; Sun, Z. Combined effects of stress, gas adsorption, and temperature on the evolution of coal seam permeability and slippage effect. *ACS Omega* **2023**, *8*, 39376–39389.
18. Liu, Y.; Zhang, Z.; Wei, X.; Shen, K.; Ba, Q. The Influence of the Injected Water on the Underground Coalbed Methane Extraction. *Energies* **2020**, *13*, 1151.
19. Fan, Z.; Fan, G.; Zhang, D.; Zhang, L.; Zhang, S.; Liang, S.; Yu, W. Optimal injection timing and gas mixture proportion for enhancing coalbed methane recovery. *Energy* **2021**, *222*, 119880.
20. Ni, X.; Zhao, Z.; Wang, Y.; Wang, L. Optimisation and application of well types for ground development of coalbed methane from no. 3 coal seam in shizhuang south block in Qinshui basin, Shanxi province, China. *J. Pet. Sci. Eng.* **2020**, *193*, 107453.
21. Liu, Y.; Zhang, Z.; Xiong, W.; Shen, K.; Ba, Q. The influence of the injected water on the underground coalbed methane extraction. *Energies* **2020**, *13*, 1151.
22. Mwakipunda, G.C.; Wang, Y.; Mgimba, M.M.; Ngata, M.R.; Alhassan, J.; Mkono, C.N.; Yu, L. Recent Advances in Carbon Dioxide Sequestration in Deep Unmineable Coal Seams Using CO2-ECBM Technology: Experimental Studies, Simulation, and Field Applications. *Energy Fuels* **2023**, *37*, 17161–17186.
23. Fan, Z.; Fan, G.; Zhang, D.; Zhang, L.; Zhang, S.; Liang, S.; Yu, W. Optimal injection timing and gas mixture proportion for enhancing coalbed methane recovery. *Energy* **2021**, *222*, 119880.
24. Yan, L.; Wen, H.; Jin, Y.; Guo, J.; Liu, Y.; Fan, S. Fluid–Solid Coupling Characteristics of Methane-Containing Coal during Borehole Extraction of Coalbed: Numerical Modeling and Experimental Research. *ACS Omega* **2023**, *8*, 49334–49346.
25. Fan, Y.; Huo, Z.; Wang, Y. Numerical simulation of CO_2-ECBM based on fluid-solid-thermal coupled model. *Saf. Coal Mines* **2022**, *53*, 162–169.

 doi:10.20944/preprints202604.1030.v1

26. Sun, Z.; Wu, K.; Shi, J.; Li, Y.; Jin, T.; Li, Q.; Li, X. Novel prediction methods for under-saturated coalbed methane wells: Effect of drainage schedules. *J. Pet. Sci. Eng.* **2019**, *181*, 106215.
27. Fang, H.; Sang, S.; Liu, S. The coupling mechanism of the thermal-hydraulic-mechanical fields in CH 4 -bearing coal and its application in the CO_2-enhanced coalbed methane recovery. *J. Pet. Sci. Eng.* **2019**, *181*, 106177.
28. Fan, Y.; Deng, C.; Zhang, X.; Li, F.; Wang, X.; Qiao, L. Numerical study of CO_2-enhanced coalbed methane recovery. *Int. J. Greenh. Gas Control.* **2018**, *76*, 12–23.
29. Liu, Q.; Cheng, Y.; Zhou, H.; Guo, P.; An, F.; Chen, H. A Mathematical Model of Coupled Gas Flow and Coal Deformation with Gas Diffusion and Klinkenberg Effects. *Rock Mech. Rock Eng.* **2015**, *48*, 1163–1180.
30. Guo, Y.; Li, S.; Qin, X.; Lu, C.; Wu, D.; Liu, L.; Zhang, N. Enhanced gas production from low-permeability hydrate reservoirs based on embedded discrete fracture models: Influence of branch parameters. *Energy* **2023**, *282*, 128886.
31. Ye, H.; Wu, X.; Li, D.; Jiang, Y. Numerical simulation of productivity improvement of natural gas hydrate with various well types: Influence of branch parameters. *J. Nat. Gas Sci. Eng.* **2022**, *103*, 104630.
32. Fan, N.; Wang, J.; Deng, C.; Mu, Y.; Fan, Y. Coalbed methane extraction in multibranch horizontal wells: Evolutions of reservoir characteristics with different geometric parameters. *Energy Sources Part A Recovery Util. Environ. Eff.* **2019**, *44*, 1375–1390.
33. Song, X.; Shi, Y.; Li, G.; Yang, R.; Wang, G.; Zheng, R.; Li, J.; Lyu, Z. Numerical simulation of heat extraction performance in enhanced geothermal system with multilateral wells. *Appl. Energy* **2018**, *218*, 325–337.
34. Zhang, H.; Liu, J.; Elsworth, D. How sorption-induced matrix deformation affects gas flow in coal seams: A new FE model. *Int. J. Rock Mech. Min. Sci.* **2008**, *45*, 1226–1236.
35. Liu, C.; Yu, B.; Zhao, H.; Hong, Z.; Tian, Z.; Zhang, D.; Liu, Y. Effective stress effect and slippage effect of gas migration in deep coal reservoirs. *Int. J. Rock Mech. Min. Sci.* **2022**, *155*, 105142.